SCIENCE CHINA
Earth Sciences

•RESEARCH PAPER•

December 2021 Vol.64 No.12: 2098–2112
https://doi.org/10.1007/s11430-020-9831-3

# Response of atmospheric circulation to multiscale SST anomaly associated with Kuroshio Extension decadal variability warming in winter

Jianqi ZHANG[1], Chongyin LI[1,2*] & Chao ZHANG[1]

[1] *College of Meteorology and Oceanography, National University of Defense Technology, Changsha 410073, China;*
[2] *LASG, Institute of Atmospheric Physics, Chinese Academy of Sciences, Beijing 100029, China*

Received November 30, 2020; revised June 29, 2021; accepted August 18, 2021; published online November 15, 2021

**Abstract** The response of atmospheric circulation to sea surface temperature anomaly (SSTA) of different scales in extratropical oceans has always been a popular issue in air-sea interactions, especially regarding the influence of widely active, small-scale ocean eddies on the atmosphere. Based on the regional climate model RegCM4.6, three sets of ensemble experiments with different initial values were designed, and the response of atmospheric circulation and possible mechanisms to Kuroshio Extension Decadal Variability SSTA with different scales (KEDV-induced SSTA) during winter were discussed. The response of atmospheric circulation to the KEDV-induced mesoscale SSTA presents a broadly tripolar pattern, while the response to the KEDV-induced large-scale SSTA presents a baroclinic structure in the central Pacific and a dipole-type response with a barotropic structure in the eastern Pacific. Further diagnostic analysis shows that under the influence of mesoscale SSTA, transient eddy activity is strengthened, and feedback of transient eddy plays a major role in the large-scale circulation anomaly in the central-eastern Pacific. The associated barotropic energy conversion also plays an important role in maintaining the large-scale circulation anomaly in the northwestern Pacific Ocean. Under the influence of large-scale SSTA, diabatic heating is stronger, and the feedback of diabatic heating plays a major role in the large-scale circulation anomaly.

**Keywords** Ensemble experiments, Kuroshio Extension, Different scales, Transient eddy feedback, Diabetic heating

**Citation:** Zhang J, Li C, Zhang C. 2021. Response of atmospheric circulation to multiscale SST anomaly associated with Kuroshio Extension decadal variability warming in winter. Science China Earth Sciences, 64(12): 2098–2112, https://doi.org/10.1007/s11430-020-9831-3

## 1. Introduction

For a long time, the response of the atmosphere to the extratropical sea surface temperature anomaly (SSTA) has been considered insignificant, and the forcing of the atmosphere on the ocean is predominant in extratropical regions (Frankignoul et al., 1997; Alexander et al., 2002). However, the results of numerical simulation and observation data in recent years show that the SSTA in extratropical regions can also significantly affect the atmosphere on the interdecadal time scale (Peng and Whitaker, 1999; Liu et al., 2006; Fang and Yang, 2016; Révelard et al., 2018), especially because different scales of SSTA can force an atmospheric response (Ma et al., 2015, 2017; Zhang et al., 2020). The Kuroshio Extension (KE) is the most active area of air-sea interaction in the North Pacific Ocean, and the KE jet has interdecadal variability from a stable state to an unstable state (Qiu and Chen, 2005; Taguchi et al., 2007; Qiu et al., 2014). At the same time, SSTA of different scales coexist in this sea area. The atmosphere has a significant response to KE interdecadal variability-induced SSTA (KEDV-IS). The observation results show that the North Pacific storm track will move along with the interdecadal variability of the KE, and its intensity will also change (Joyce et al., 2009; O'Reilly and

* Corresponding author (email: lcy@lasg.iap.ac.cn)

Czaja, 2015). This change is directly related to the baroclinicity of the lower atmosphere, and strong baroclinicity is often associated with an anchored storm track near the ocean front (Sampe et al., 2010; Yao et al., 2016). The response of large-scale circulation to KEDV-IS shows a wide range of tripolar pattern responses, similar to NPO/WP (North Pacific oscillation/West Pacific teleconnection) (Révelard et al., 2016), in which the nonlinear feedback of transient eddies plays an important role. Whether the numerical model can correctly reproduce the barotropic structural response of the atmosphere to SSTA in the extratropical region depends on whether the model can better simulate the response of synoptic transient eddy anomalies, which is directly related to the baroclinicity in the lower atmosphere. The basin-scale ocean front in KEDV-IS is the key to influencing the baroclinicity in the lower atmosphere, which can anchor the storm track significantly near the ocean front (Nakamura et al., 2004; Minobe et al., 2008; Taguchi et al., 2012). In addition, it is also noted that KEDV-IS are accompanied not only by large-scale SSTA (KEDV-L and KEDV induced large-scale SSTA) but also by abundant mesoscale SSTA (KEDV-M and KEDV induced mesoscale SSTA) (Qiu and Chen, 2005; Cheng et al., 2014; Liu et al., 2020), where the most active mesoscale ocean eddies exist in the North Pacific Ocean. Mesoscale SSTA can influence the atmospheric boundary layer by influencing SST. Satellite observation data and sea surface wind field data show that the wind speed on the warm mesoscale SSTA increases and that on the surface of the cold mesoscale SSTA decreases, which is explained by the "vertical mixing mechanism" (Wallace et al., 1989). It can also be observed that there is strong convergence of the wind field on the surface of the warm mesoscale SSTA and divergence of the wind field on the surface of the cold mesoscale SSTA. Therefore, there is also an explanation of the "air pressure adjustment mechanism" (Lindzen and Nigam, 1987). In addition, the mesoscale SSTA can enhance the water vapor content in the atmosphere and can influence the upper atmosphere through latent heat release. Mesoscale SSTA can also have an obvious influence on storm tracks and large-scale circulation (Foussard et al., 2018). Using numerical models with different resolutions, it is found that the high-resolution numerical model can better reflect the mesoscale SSTA, thus enhancing the storm track and large-scale circulation response (Ma et al., 2015, 2017; Zhang et al., 2020). Mesoscale oceanic stochastic forcing can improve the simulated atmospheric response by generating more organized atmospheric transient eddies (Sun et al., 2018). Mesoscale SSTA can have a significant influence on weather and climate. In the past, attention has been given to the influence of KEDV-IS on large-scale atmospheric circulation, but the effect of different-scale SSTA of the KE on atmospheric circulation, especially the widely active mesoscale SSTA, is not understood. Therefore, its influence on the interdecadal atmospheric circulation anomaly urgently needs to be revealed.

## 2. Data, method, and numerical experiment

### 2.1 Data

(1) The SST data used in this paper come from the monthly mean optimal interpolation dataset provided by the National Oceanic and Atmospheric Administration (NOAA), with a resolution of 0.25°×0.25°. The time period is from 1993 to 2012.

(2) Sea surface height anomaly (SSHA) provided by the AVISO (Archiving Validation and Interpretation of Satellite Oceanographic) Center in France is used to calculate the monthly mean Kuroshio Extension index, with a resolution of 0.25°×0.25° (Ducet et al., 2000). The time period is from January 1993 to December 2012.

(3) The data of initial values and boundaries used in RegCM4.6 are from the National Centers for Environmental Prediction-National Center for Atmospheric Research (NCEP/NCAR), and the resolution is 0.25°×0.25° (Kalnay et al., 1996).

### 2.2 Method

(1) In this paper, the KE index (KEI) defined by Qiu et al. (2014) is used, which is obtained by the monthly average SSHA in the interval (31°N–36°N, 140°E–165°E) as the monthly average KEI. The monthly average and normalized KEI during the winter periods in a 20-year interval (1993–2012) are shown in Figure 1a, and it can be found that the KEI shows obvious interdecadal variation characteristics. Because the interaction between sea and air is most intense in early winter and deep winter, winter in this paper is defined as occurring from October to January of the following year (October, November, December, and January, ONDJ). The SST regressed by the monthly average KEI in winter is shown in Figure 1b. In the KE stable state, there is large-scale SSTA warming in the central part of the North Pacific Ocean, and the SSTA in the northern and eastern parts of the North Pacific Ocean becomes significantly colder. This SSTA type represents the KEDV-IS. At the same time, there is abundant mesoscale SSTA.

(2) We use the Loess spatial filter to separate the SSTA warming region (30°N–40°N, 140°E–170°W), where the KE has the most significant influence on the mesoscale and large-scale parts. The results are shown in Figure 1c and 1d. The mesoscale SSTA separated by the Loess spatial filter is characterized by the alternating distribution of cold eddies and warm eddies, which is the KE mesoscale SSTA (KEDV-M). The large-scale SSTA separated by the spatial filter

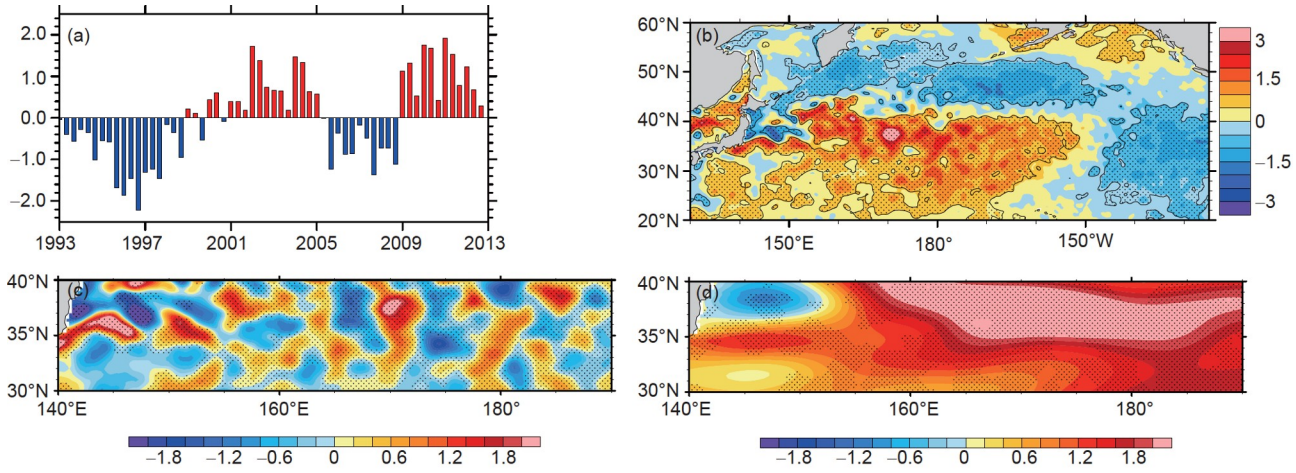


**Figure 1** (a) Cold season (ONDJ) KEI from 1993 to 2012; (b) the SST field is regressed onto the KEI; (c) KEDV-M (°C, shading); (d) KEDV-L (°C, shading). Statistically significant differences at 90% according to Student's *t* test are stippled.

shows large-scale SSTA warming east of 150°E.

### 2.3 Numerical experiment

The regional climate model RegCM4.6 (Giorgi et al., 2012) is used in this paper, which has been widely used in regional climate simulation and prediction after many years of development. The model uses the Zeng scheme of sea surface flux (Zeng et al., 1998). The boundary layer uses the nonlocal diffusion Holtslag boundary layer scheme (Holtslag and Boville, 1993), and the cumulus convection parameterization scheme adopts the convective mass flux Tiedtke scheme. The horizontal resolution of the model is 0.3°×0.3°, and it is divided into 23 layers vertically. The model simulation area covers the entire North Pacific (120°E–140°W, 20°N–80°N), and the central grid point is located at (45°N, 180°).

There are three groups of experiments with different initial values, and each group contains 16 members (Table 1). The difference between the three groups of tests is the different forcing of SSTA on the surface. The first group of experiments is the control test (named the CTRL test), and the SST field used is the monthly average climatological SSTA of multiple years (1993–2012) as the underlying surface SSTA field. The second test is sensitivity test 1 (named the KSTS test), and the underlying surface SST is based on the monthly average SST field in the climatic state for many years. The warming part of the KEDV-IS (140°E–160°W, 32°N–40°N) is superimposed on the climatological SSTA as the underlying surface forcing in the second experiment. The third test is sensitivity test 2 (MEFS). Based on the monthly average SST in the climatic state, the large-scale SSTA with the KEDV-L in the interval (140°E–160°W, 32°N–40°N) is superimposed on the climatological SSTA, which is used as the underlying surface SST field in the third test. In the above experiments, when the SSTA is superimposed, the false discontinuity at the boundary is processed by a smoothing function many times, which causes it to be closer to the real SST field. The numerical test time integral is from 00:00 on September 1st to 18:00 on February 2nd of the following year, and the first month is the spin-up time. The initial conditions of each set member are from September 1st in 1981, 1982, 1985, 1986, 1989, 1990, 1997, 1998, 2000, 2001, 2002, 2003, 2004, 2005, 2006, and 2007. The boundary condition of all tests is the boundary condition of the climate state every 6 h, which is the atmospheric reanalysis data with an average interval of 6 h in 30 years (1981–2010). The results of the differences between the two groups represent different meanings. For example, the KSTS-CTRL represents the response of the atmosphere to the KEDV-IS, KSTS-MEFS represents the response of the mesoscale SST anomaly KEDV-M, and MEFS-CTRL represents the response of the atmosphere to the large-scale SST anomaly KEDV-L.

Additionally, we used Student's *t* test to test for significance. The hypothesis of the significance test was that sensitivity experiment 1 using the climatology SST superimposed on the KE-related SSTA would not significantly differ from control experiment 2 using the climatology SST. A total of 16 members of each ensemble experiment were used.

There are $n_1$=16 winter cold seasons in experiment 1 and $n_2$=16 winter cold seasons in experiment 2. The numbers $n_1$ and $n_2$ are used as the independent sample sizes. The mean values of the meteorological element $x$ of the two sample groups we calculated are $x^s$ and $x^c$. The null hypothesis is that the average of the two samples has no significant differences, and the statistic $t$ follows a $t$ distribution with $n_1+n_2-2$ degrees of freedom. $s^2$ denotes the unbiased estimator of the variance of the difference. $\overline{x^c}$ and $\overline{x^s}$ denote the winter mean value of each of the two winter experiments, respectively.

$$t=\frac{\overline{x^s}-\overline{x^c}}{s\sqrt{\frac{1}{n_1}+\frac{1}{n_2}}}. \quad (1)$$

The calculation of $s^2$ is

$$s^2=\frac{\sum_{i=1}^{n_1}(x_i^s-\overline{x^s})^2+\sum_{i=1}^{n_2}(x_i^c-\overline{x^c})^2}{n_1+n_2-2}. \quad (2)$$

For a given significance level and degrees of freedom $n_1+n_2-2$, we can find the corresponding critical value $t_\alpha$. According to Student's $t$-distribution table, if $|t|<t_\alpha$, we accept the hypothesis; if not, we reject the hypothesis. The statistical significance of the differences between each pair of simulations was estimated with Student's $t$ test at a 90% confidence level.

### 2.4 Verification of numerical model

The results of previous statistical analysis show that the response of large-scale atmospheric circulation to the KEDV-IS presents a wide range of tripolar structures. For example, Révelard et al. (2016) used the KEI, which was 1–2 months ahead of the atmosphere, and after removing the influence of ENSO, they demonstrated that the response showed a tripolar structure with an equivalent barotropic structure. There are significant positive geopotential height anomalies in the northwestern North Pacific and the eastern North Pacific near the west coast of the North American continent, while there are extensive negative geopotential height anomalies in the Gulf of Alaska and in the north. Numerical test results show that the response of the atmosphere to the KEDV-IS also shows a similar tripolar structure response, as shown in Figure 2. In the upper troposphere, a positive geopotential height anomaly appeared in the western North Pacific and the eastern North Pacific near 40°N, while a negative geopotential height anomaly appeared over Alaska. The response of the lower atmosphere also presents a tripolar structure. The difference is that the positive anomaly center of the geopotential height in the western North Pacific is near the Kamchatka Peninsula; therefore, the geopotential height response of the western North Pacific shows a baroclinic structure westward and southward tilt with height. These results are also more consistent with the results of a previous analysis (Révelard et al., 2016). This confirms that the KEDV can indeed have a profound impact on large-scale atmospheric circulation and confirms that the numerical model can simulate this response more accurately.

## 3. The response of the atmosphere to large-scale SSTA

### 3.1 The response of large-scale circulation

We mainly focus on the response of atmospheric circulation to different scales of the KEDV, as shown in Figure 3. The geopotential height of 250 hPa manifests as a dipolar pattern in the eastern North Pacific, which is positive in the south and negative in the north. The geopotential height of 850 hPa has a similar pattern, but the positive geopotential height anomaly in the south is much weaker. There are some positive geopotential height anomalies in the upper level but some negative anomalies in the lower level near 180° in the central North Pacific, which presents a weak baroclinic structure.

### 3.2 Possible mechanisms

#### *3.2.1 The feedback of the high frequency of synoptic transient eddies*

For the response of atmospheric circulation to the KEDV-L, the SSTA impacts the large-scale SSTA by inducing more diabetic heating, and the meridional gradient of the SSTA can alter the baroclinicity in the lower atmosphere, which can induce more synoptic transient eddies. The feedback of transient eddies may be the main factor that maintains the response of atmospheric large-scale circulation to the KEDV-L (Nakamura et al., 1987; Lau, 1988; Lau and Nath, 1991). The feedback of synoptic eddies can transform the baroclinic structure of the atmosphere into a barotropic structure (Peng and Whitaker, 1999; Fang and Yang, 2016). However, we can also note that the response of the vertical gradient of diabetic heating to the KEDV-L can also maintain the baroclinic structure (Tao et al., 2020). The quasi-geostrophic potential vorticity (QGPV) equation can provide some analysis, which consists of diabetic heating and transient eddy forcing as follows (Fang and Yang, 2016):

$$\left(\frac{\partial}{\partial t}+\mathbf{V}_h\cdot\nabla\right)\left[\frac{1}{f}\nabla^2\bar{\phi}+f+\frac{\partial}{\partial p}\left(\frac{f}{\sigma_1}\frac{\partial\bar{\phi}}{\partial p}\right)\right]$$
$$=-f\frac{\partial}{\partial p}\left(\frac{\alpha}{\sigma_1}\frac{\overline{Q}_d}{\overline{T}}\right)-f\frac{\partial}{\partial p}\left(\frac{\alpha}{\sigma_1}\frac{\overline{Q}_{\text{eddy}}}{\overline{T}}\right)+\overline{F}_{\text{eddy}}, \quad (3)$$

where $\phi$ is the geopotential height, $f$ is the Coriolis force parameter, $\alpha$ is the reciprocal of air density, and $\sigma_1$ is the static stability parameter. $T$ is the temperature, $\mathbf{V}_h$ is the geostrophic wind, and the overbar denotes the winter mean. $\overline{Q}_d$ is winter-mean diabatic heating. $\overline{Q}_{\text{eddy}}$ is winter-mean transient eddy heating, which is as follows:

$$\overline{Q}_{\text{eddy}}=-\nabla\cdot\overline{\mathbf{V}_h'T'}-\frac{\partial\overline{\omega'T'}}{\partial p}+\frac{R}{C_p p}\overline{\omega'T'}. \quad (4)$$

In the equation, the prime denotes synoptic-scale (2–8 days) disturbances by the Lanzcos bandpass filter. $\omega$ is the vertical velocity in the $p$ coordinate, $R$ is the gas constant for dry air, and $C_p$ is the specific heat of dry air at a constant pressure. $F_{\text{eddy}}$ is the transient eddy vorticity forcing; that is, $\overline{F}_{\text{eddy}}=-\nabla\cdot\overline{\mathbf{V}_h'\zeta'}$, and $\zeta$ is the relative vorticity. $F_{\text{eddy}}$ in-

**Table 1** Three sets of ensemble numerical experiments (16 members) using the RegCM4.6 model[a)]

| Experiment name | Initial field | Lateral boundary condition |
|---|---|---|
| Control simulation (CTRL) | Climatology SST of each month and atmospheric initial field from 1 September in 16 different years | Climatological (1981–2010) 6-hour NCEP2 reanalysis data |
| KEDV-induced SSTA simulation (KSTS) | Climatology of each month (but KE-related SSTA in the KE region) and atmospheric initial field from 1 September in 16 different years | Climatological (1981–2010) 6-hour NCEP2 reanalysis data |
| Mesoscale filtered simulation (MEFS) | Climatology of each month (but KE-related large-scale SSTA in the KE region) and atmospheric initial field from 1 September in 16 different years | Climatological (1981–2010) 6-hour NCEP2 reanalysis data |

a) The integration time is (00 UTC 01 September to 18 UTC 2 February), and the atmospheric (oceanic) resolution is 0.3°×0.3° (0.25°×0.25°)

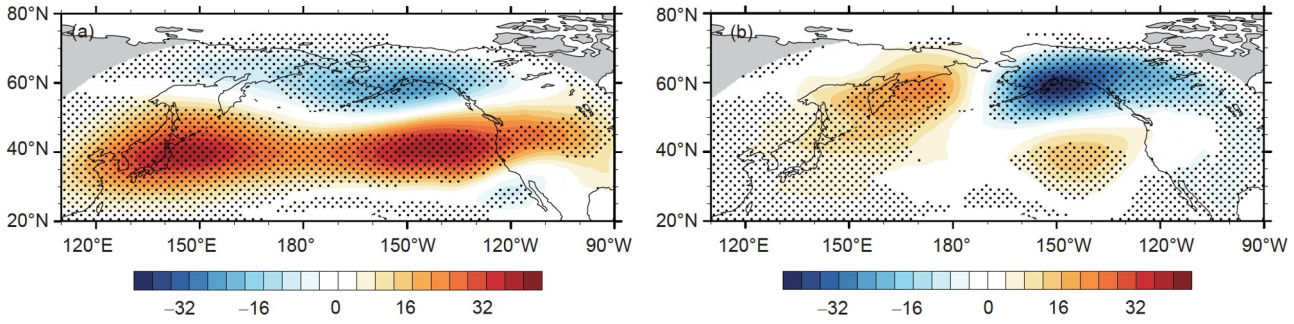


**Figure 2** The response of geopotential height to the KEDV-IS (shaded, unit: m) (KSTS-CTRL). (a) Response of geopotential height to the KEDV-IS at 250 hPa; (b) response of geopotential height to the KEDV-IS at 925 hPa. Statistically significant differences at 90% according to Student's *t* test are stippled.

dicates the transportation of divergence of transient eddy flux. Regarding the tendency of geopotential height, which consists of the above terms as eq. (5), inverting $\left(\frac{1}{f}\nabla^2+\frac{f}{\sigma_1}\frac{\partial^2}{\partial p^2}\right)$ by using successive overrelaxation (SOR) on eq. (5) (Hadjidimos, 2000), we can obtain the tendency of geopotential height forcing by terms of transient eddy heating $F1$, terms of transient eddy vorticity forcing $F2$, and terms of diabatic heating $F3$:

$$\left(\frac{1}{f}\nabla^2+\frac{f}{\sigma_1}\frac{\partial^2}{\partial p^2}\right)\left(\frac{\partial\Delta\bar{\phi}}{\partial t}\right) = \underbrace{-f\frac{\partial}{\partial p}\left(\frac{\alpha}{\sigma_1}\frac{\Delta\overline{Q}_{\text{eddy}}}{\overline{T}}\right)}_{F1}+\underbrace{\Delta F_{\text{eddy}}}_{F2} \underbrace{-f\frac{\partial}{\partial p}\left(\frac{\alpha}{\sigma_1}\frac{\Delta\overline{Q}_{d}}{\overline{T}}\right)}_{F3}, \quad (5)$$

where Δ denotes the winter-mean response to the KEDV-L. In the process of numerical solution, the boundary condition is set according to Lau and Holopainen (1984). Under the influence of the KEDV-L, the SOR method is applied to eq. (5), and the results are shown in Figure 4. We find that the feedback of $F1$ on geopotential height is mainly in the eastern North Pacific. As shown in Figure 4a and 4b, there are some positive anomalies south of 40°N in the eastern North Pacific, which have a positive contribution to the positive geopotential height anomaly. The feedback of $F1$ on the geopotential height anomaly is much weaker in the lower atmosphere in the eastern North Pacific. The feedback of $F2$ on the geopotential height anomaly manifests as a saddle field with a barotropic structure. As shown in Figure 4c and 4d, the feedback with positive feedback in the south and negative feedback in the north structure is consistent with the geopotential height anomaly in the eastern North Pacific. This indicates that the feedback of terms $F2$ makes a positive contribution to the geopotential height anomaly in the eastern North Pacific. We can also notice that the feedback of $F2$ on the geopotential height anomaly is a negative anomaly in the central North Pacific, while the geopotential height anomaly in the central North Pacific is a weak positive anomaly; therefore, the feedback of $F2$ is not the main forcing in the central North Pacific. The feedback of $F3$ on the geopotential height anomaly is shown in Figure 4e and 4f. Diabatic heating consists of latent heat induced by cumulus convection and large-scale condensation precipitation, vertical eddy diffusion heating and radiation heating, and vertical eddy diffusion heating contains sensible heating. The feedback of $F3$ on the geopotential height anomaly is a much stronger positive anomaly in the KE region and central North Pacific in the upper level, while it is a much weaker anomaly in the lower atmosphere, which manifests as a baroclinic structure. This may be the main contribution to the geopotential height anomaly with a weak baroclinic structure in the central North Pacific, which indicates that diabatic heating is very important under the influence of the KEDV-L.

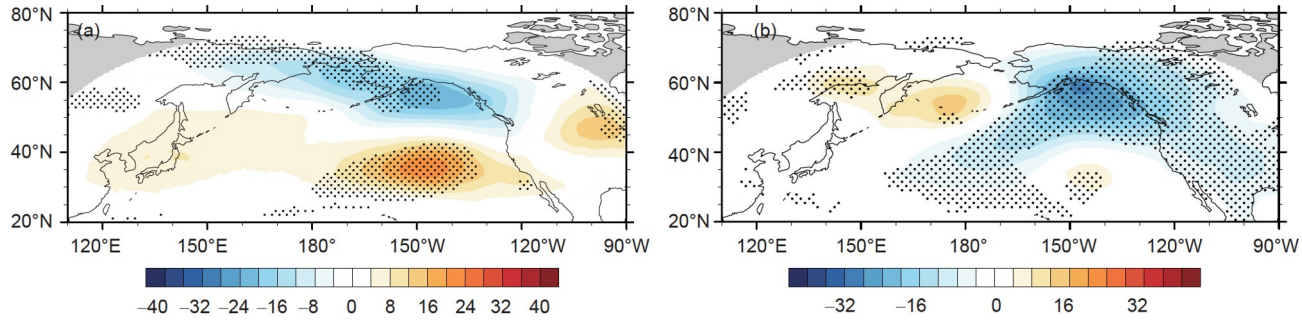


**Figure 3** Response of the geopotential height field to the KEDV-L (shading, unit: m) (MEFS-CTRL). (a) Responses of 250 hPa geopotential height to the KEDV-L; (b) the response of 850 hPa geopotential height to the KEDV-L. Statistically significant differences at 90% according to Student's *t* test are stippled.

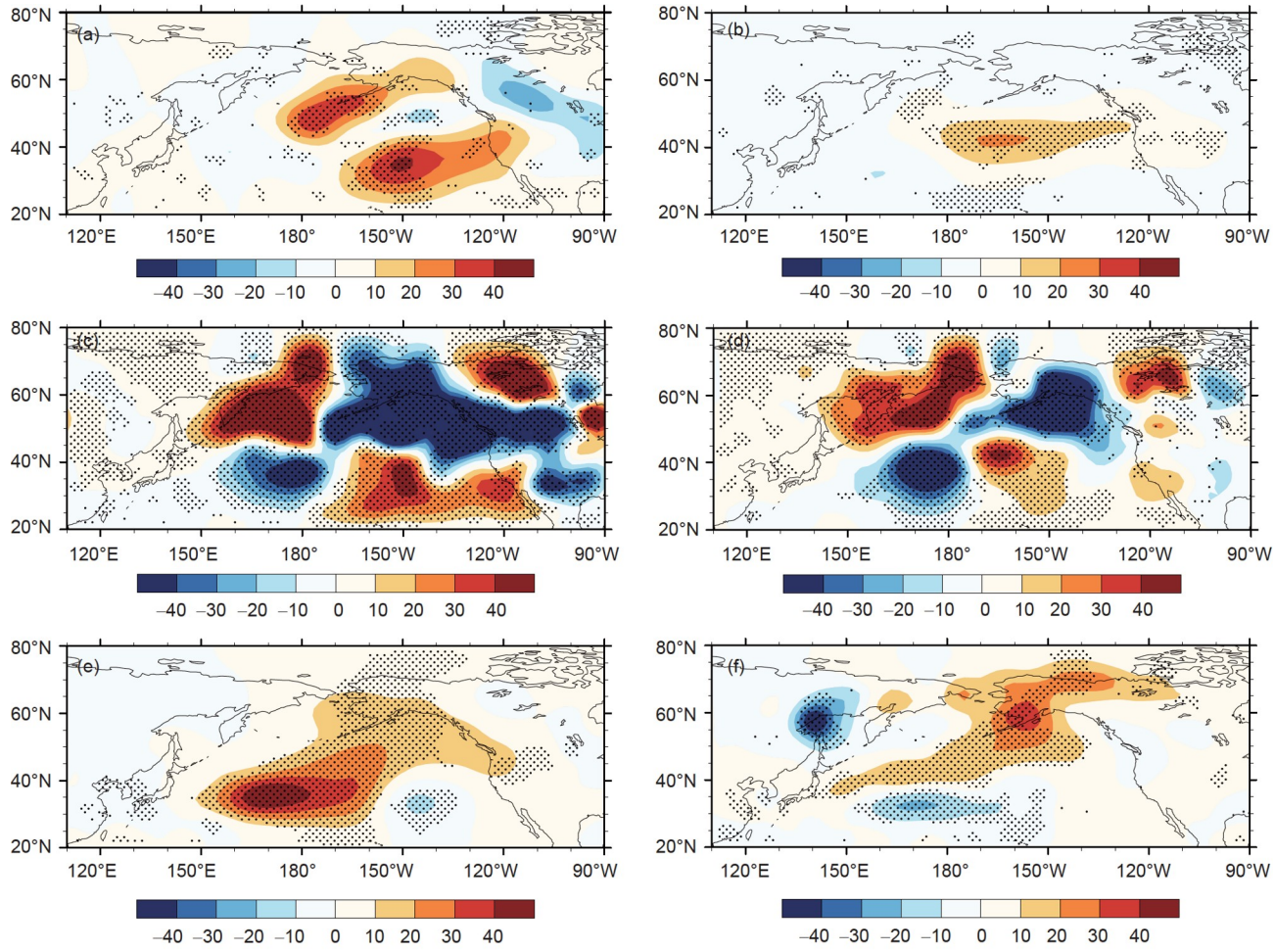


**Figure 4** Response of transient eddy heating to KEDV-L feedback on the geopotential height field at 250 hPa (a) and 850 hPa (b) (shading, unit: $10^{-5}$ m$^2$ s$^{-3}$). Response of transient eddy vorticity to KEDV-L feedback on the geopotential height field at 250 hPa (c) and 850 hPa (d). Response of diabatic heating to KEDV-L feedback on the geopotential height field at 250 hPa (e) and 850 hPa (f) (shading, unit: $10^{-5}$ m$^{-2}$ s$^{-3}$). Statistically significant differences at 90% according to Student's *t* test are stippled.

*3.2.2 Barotropic energy and baroclinic energy conversion*

From the above, we mainly focus on the feedback of high-frequency synoptic transient eddies on atmospheric circulation. The winter-mean response of the atmospheric circulation anomaly can be considered a seasonal-scale, low-frequency disturbance. This low-frequency disturbance can be maintained by absorbing energy through interactions with the basic climatological flow. Many studies have shown that the similar NPO/WP pattern can be sustained by absorbing energy through barotropic energy or baroclinic energy conversion from basic climatological flow (Hoskins et al., 1985; Nakamura et al., 1987). The calculations of barotropic energy and baroclinic energy conversion are as follows:

$$\mathrm{TE}=\frac{v'^2-u'^2}{2}\left(\frac{\partial u_c}{\partial x}-\frac{\partial v_c}{\partial y}\right)-u'v'\left(\frac{\partial u_c}{\partial y}+\frac{\partial v_c}{\partial x}\right), \tag{6}$$

$$\mathrm{TP}=\frac{R}{pS_p}\left(-u'T'\frac{\partial T_c}{\partial x}-v'T'\frac{\partial T_c}{\partial y}\right), \tag{7}$$

where $u$ represents zonal wind, $v$ represents meridional wind, and $S_p=(R/p)\left[\left(RT_c/pC_p\right)-\left(\mathrm{d}T_c/\mathrm{d}p\right)\right]$. The prime in the above equation represents the low frequency of seasonal scale disturbance, and the lower corner marker $c$ represents the climatological seasonal mean, which is the result of the climatological ensemble experiment CTRL.

In the above equation, when the TE is positive, it represents the transformation of kinetic energy from basic climatological flow to low-frequency mode, and vice versa. When the TP is positive, it represents the transformation of available potential energy from basic climatological flow to low-frequency mode, and vice versa. Under the influence of the KEDV-L, the results of barotropic energy conversion are shown in Figure 5a and 5b, and we find that the barotropic energy conversion at 250 hPa mainly lies south of 40°N in the central North Pacific. In this region, the kinetic energy is from basic climatological flow to low-frequency mode, which has a weak contribution to the low-frequency mode in the eastern North Pacific. The barotropic energy conversion at 850 hPa has a nonsignificant signal. The baroclinic energy conversion is calculated as Figure 5c and 5d, and we find that the baroclinic energy conversion at 850 or 250 hPa mainly lies in the central North Pacific, which has a weak contribution to the low frequency in the eastern North Pacific.

### 3.2.3 *Energy conversion efficiency evaluation*

To evaluate the importance of feedback of a high-frequency transient eddy, diabatic heating, and energy conversion between basic climatological flow and low-frequency mode, according to Okajima et al. (2018), the energy conversion efficiency $R$ is calculated, which denotes the relative energy divided by the total energy:

$$R=\frac{E}{\mathrm{APE}+\mathrm{KE}}. \tag{8}$$

The total energy consists of eddy available potential energy (APE) and eddy kinetic energy (KE):

$$\begin{aligned}\mathrm{APE}&=\frac{R}{pS_p}\left(\frac{T'^2}{2}\right),\\ \mathrm{KE}&=\frac{u'^2+v'^2}{2}.\end{aligned} \tag{9}$$

The kinetic energy $\mathrm{CK}_H$ and available potential energy $\mathrm{CP}_H$ induced by feedback of a high-frequency transient eddy in the low-frequency mode are calculated as follows:

$$\begin{aligned}\mathrm{CK}_H=&u'\left[-\frac{\mathrm{g}}{f}\frac{\partial}{\partial y}\left(\frac{\partial\phi'}{\partial t}\right)\right]\\ &+v'\left[-\frac{\mathrm{g}}{f}\frac{\partial}{\partial x}\left(\frac{\partial\phi'}{\partial t}\right)\right],\end{aligned} \tag{10}$$

$$\mathrm{CP}_H=-\frac{\mathrm{g}}{S_p}T'\left[\frac{\partial}{\partial p}\left(\frac{\partial\phi'}{\partial t}\right)\right]. \tag{11}$$

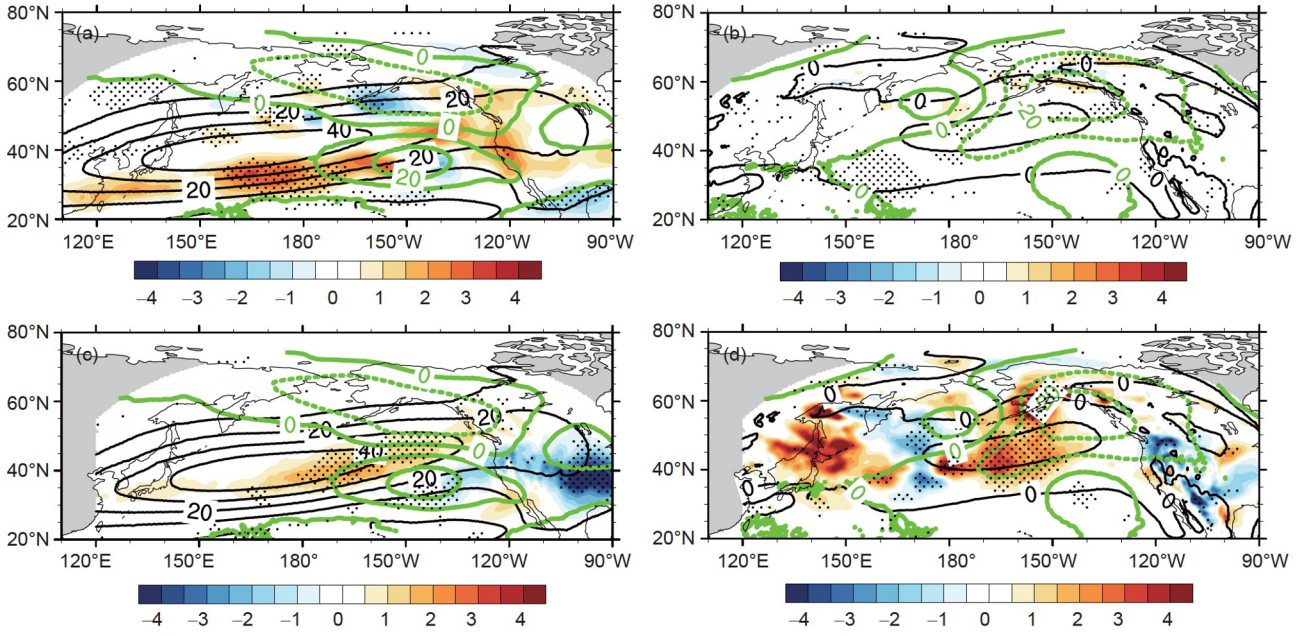


**Figure 5** Response of barotropic and baroclinic energy conversion (shaded, unit: $10^{-4}$ m$^2$ s$^{-3}$) to the KEDV-L. (a) Barotropic energy conversion at 250 hPa and (b) barotropic energy conversion at 850 hPa; (c) and (d) same as (a) and (b) but for baroclinic energy conversion. The black isoline is the climatological zonal wind (unit: m s$^{-1}$), and the green isoline is the response of geopotential height to mesoscale the SSTA (unit: m); statistically significant differences at 90% according to Student's $t$ test are stippled.

The lower corner marker *H* denotes the energy induced by feedback of a high-frequency transient eddy and diabatic heating. The prime denotes seasonal scale, low-frequency disturbance. In eq. (10), the tendency of the geopotential height anomaly $\frac{\partial \phi'}{\partial t}$ is from feedback of high-frequency transient eddy forcing and transient eddy heating, which denotes the kinetic energy of the low-frequency mode induced by feedback of the high-frequency synoptic transient eddy. The relative energy conversion is calculated as CK_en and CP_en. The tendency of the geopotential height anomaly $\frac{\partial \phi'}{\partial t}$ in eq. (11) is the result of feedback of diabatic heating, which represents the available potential energy of the low-frequency mode induced by diabatic heating. The relative energy conversion efficiency is calculated as CP_dh.

The simulation area is divided into three parts, namely, the western North Pacific (25°N–60°N, 120°E–160°E), central North Pacific (25°N–60°N, 160°E–160°W) and eastern North Pacific (25°N–60°N, 60°W–120°W). After calculating the energy conversion efficiency, regional integration is performed, and the energy conversion efficiency is shown in Figure 6. CK is the energy conversion efficiency induced by barotropic energy conversion between the low-frequency mode and basic climatological flow through eq. (6), and CP is the energy conversion efficiency induced by baroclinic energy conversion between the low-frequency mode and basic climatological flow through eq. (7). Under the influence of the KEDV-L, there is little difference in every term of energy conversion efficiency in the western North Pacific, but the energy conversion efficiency of diabatic heating is much stronger in the central North Pacific. The energy conversion efficiency of synoptic transient eddies still occupies a dominant position in the eastern North Pacific. Therefore, under the influence of the KEDV-L, feedback of diabatic heating and transient eddies plays an important role in regulating atmospheric circulation.

### 3.3 Diagnosis of secondary circulation in the latitude-altitude section

The meridional propagation of synoptic waves can induce positive feedback on atmospheric circulation, which can maintain the jet through meridional convergence of synoptic eddy momentum flux (Robinson, 2006; Gerber and Vallis, 2007). The synoptic eddy heat flux drives the baroclinicity shift to pole with secondary circulation in altitude-latitude sections (Vallis, 2006).

Under the influence of the KEDV-L, the feedback of transient eddies plays an important role in the eastern North Pacific, but has feedback of diabatic heating in the central North Pacific. From the perspective of potential vorticity, diabatic heating can cause anticyclonic potential vorticity in the upper troposphere but has cyclonic potential vorticity in the lower troposphere, thus exerting an influence on atmospheric large-scale circulation (Hoskins et al., 1985; Ahmadi-Givi, 2002). Furthermore, we can consider the baroclinic instability as the interaction between potential vorticity in the upper troposphere and lower troposphere (Hoskins et al., 1985). The above two processes can lead to different characteristics of secondary circulation in latitude-altitude sections. Under the influence of the KEDV-L, the secondary circulation in the altitude-latitude section is shown in Figure 7. We find that the cyclonic secondary circulation near peak diabatic heating occurs in the interval (30°N–40°N). North of 40°N, there is northerly wind and cold advection, which may be caused by diabatic heating.

To diagnose the possible reason for secondary circulation and to compare the difference in feedback of synoptic transient eddies and diabatic heating on large-scale circulation, we use the tendency of the zonal wind equation and continuity equation. We divide the variables into climatological

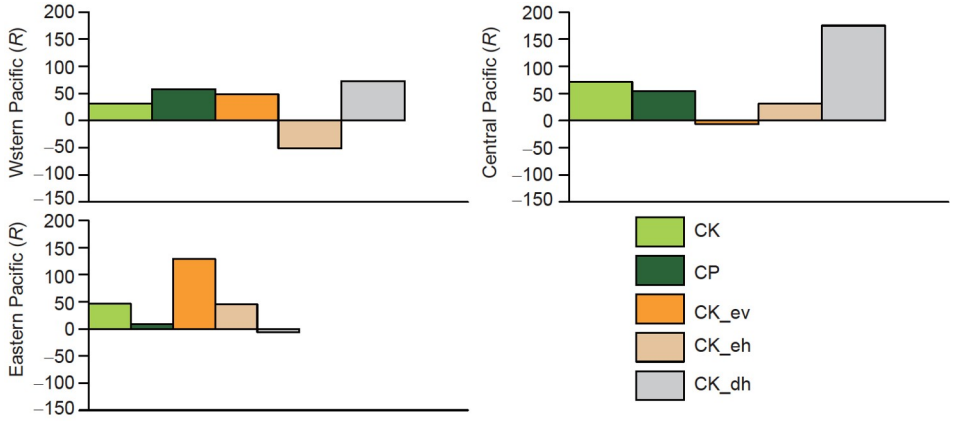


**Figure 6** Energy conversion efficiency *R*. The figure shows the barotropic energy conversion efficiency (CK), baroclinic energy conversion efficiency (CP), energy conversion efficiency caused by transient eddy vorticity feedback (CK_ev), energy conversion efficiency caused by transient eddy heating feedback (CK_eh) and energy conversion efficiency caused by diabatic heating (CP_dh) under the influence of the KEDV-L in the western Pacific, central Pacific and eastern Pacific regions.

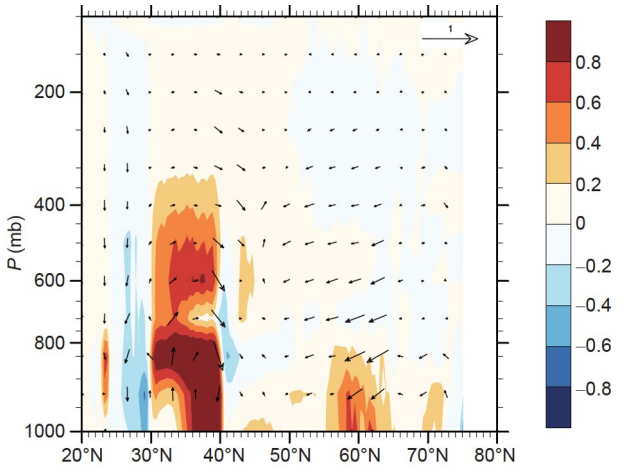


**Figure 7** The response of diabatic heating (unit: K $s^{-1}$) and circulation (vector arrows, meridional wind (unit: 10 m $s^{-1}$) and vertical velocity (unit: $10^{-2}$ m $s^{-1}$)) in latitude-altitude sections to the KEDV-L averaged at 130°E–125°W. 1 mb=100 Pa.

means and disturbances to obtain the diagnostic equation:

$$\frac{1}{f}\frac{\partial^2\chi}{\partial y^2}+\frac{f}{\sigma_1}\frac{\partial^2\chi}{\partial p^2}=\underbrace{\frac{1}{\sigma_1}\frac{\partial}{\partial p}\nabla\cdot\left(-\overline{u'v'},\frac{f}{\partial\overline{\theta}/\partial p}\overline{\theta'v'}\right)}_{1}-\underbrace{\frac{R}{\sigma_1 f p C_p}\frac{\partial\overline{Q_d}}{\partial y}}_{2}, \tag{12}$$

$$\overline{v}=-\frac{\partial\chi}{\partial p},\ \overline{\omega}=\frac{\partial\chi}{\partial y}. \tag{13}$$

In the above equation, the prime denotes a synoptic scale (2–8 d) by filter bandpass, and the overbar denotes the winter mean. $\chi$ is the stream function, $\theta$ is the potential temperature, $(\overline{v},\overline{\omega})$ is the meridional and vertical wind, respectively, and $Q_d$ is diabatic heating. Eq. (12) contains the transportation of momentum flux and heat flux by synoptic eddies, which reflect the function of the EP flux (Eliassen-Palim flux) (Eliassen and Palm, 1960); it is a vector representing the transportation of heat and momentum by synoptic eddies.

The numerical solution of nonlinear Poisson equations with boundary conditions ($\overline{v}=0$ in the northern and southern boundaries and $\overline{\omega}=0$ in the upper and lower boundaries) is shown in Figure 8. We find that under the influence of the KEDV-L, the vertical gradient of divergence of the EP flux can induce weak anticlockwise secondary circulation, as shown in Figure 8a, but also especially clockwise secondary circulation and northerly wind north of 40°N induced by diabatic heating, as shown in Figure 8b, which resemble the secondary circulation in the altitude-latitude section. Therefore, the feedback of diabatic heating may be the main reason for the clockwise secondary circulation in the altitude-latitude section, which plays a more important role under the influence of the KEDV-L.

## 4. The response of the atmosphere to mesoscale SSTA

### 4.1 The response of large-scale circulation

The response of atmospheric circulation to the KEDV-M is shown in Figure 9. We find that the response of the geopotential height anomaly to the KEDV-M resembles the response of the geopotential height anomaly to the KEDV-IS; that is, the positive geopotential height anomaly in the western North Pacific and eastern North Pacific near the west coast of the North American continent at 250 hPa. At 850 hPa, there is a positive geopotential height anomaly in the eastern North Pacific, but the positive anomaly is much weaker in the western North Pacific and manifests as a baroclinic structure from the lower troposphere to the upper troposphere.

### 4.2 Possible mechanisms

*4.2.1 The feedback of the high-frequency synoptic transient eddy*

Using the SOR method on eq. (5), the feedback of synoptic

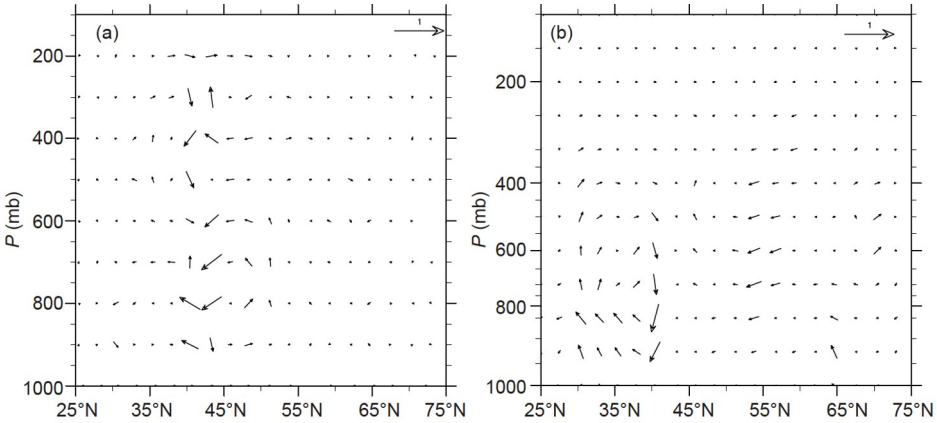


**Figure 8** Latitude-altitude section secondary circulation (meridional velocity (unit: 10 m $s^{-1}$) and vertical velocity (unit: $10^{-2}$ m $s^{-1}$)) caused by eddy momentum and eddy heat flux (a) and diabatic heating (b) under the influence of the KEDV-L.

transient eddies on geopotential height anomalies is shown in Figure 10. We find that the feedback of $F1$ on geopotential height is negative in the central-eastern North Pacific north of 40°N and the Gulf of Alaska, but it is positive in the eastern North Pacific near 40°N and south of 40°N, which contributes to the geopotential height anomaly in the eastern North Pacific. However, in the lower troposphere, especially in the KE region, the feedback of $F1$ is positive and manifests as a baroclinic structure. The feedback of $F2$ on geopotential height is positive with a barotropic structure in the KE region, central-eastern North Pacific and west coast of the North American continent, but the stronger signal is

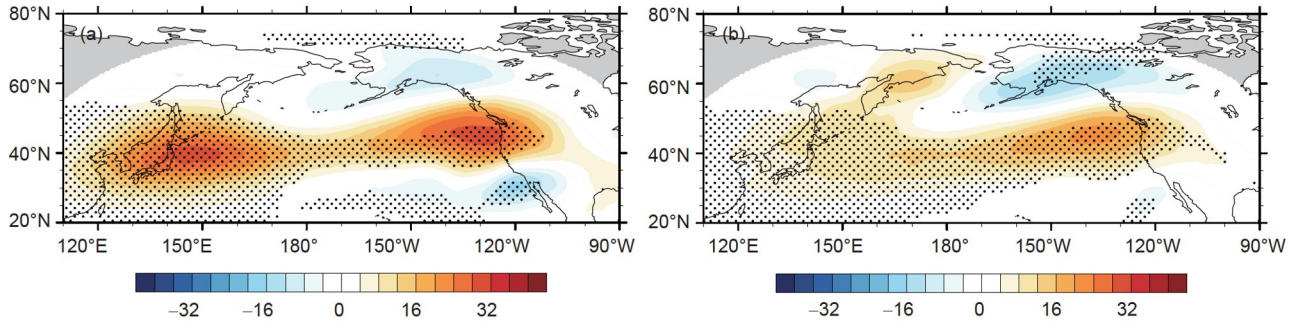


**Figure 9** Response of the geopotential height field to the KEDV-M (shading, unit: m) (KSTS-MEFS). (a) Responses of 250 hPa geopotential height to the KEDV-M; (b) the response of 850 hPa geopotential height to the KEDV-M. Statistically significant differences at 90% according to Student's $t$ test are stippled.

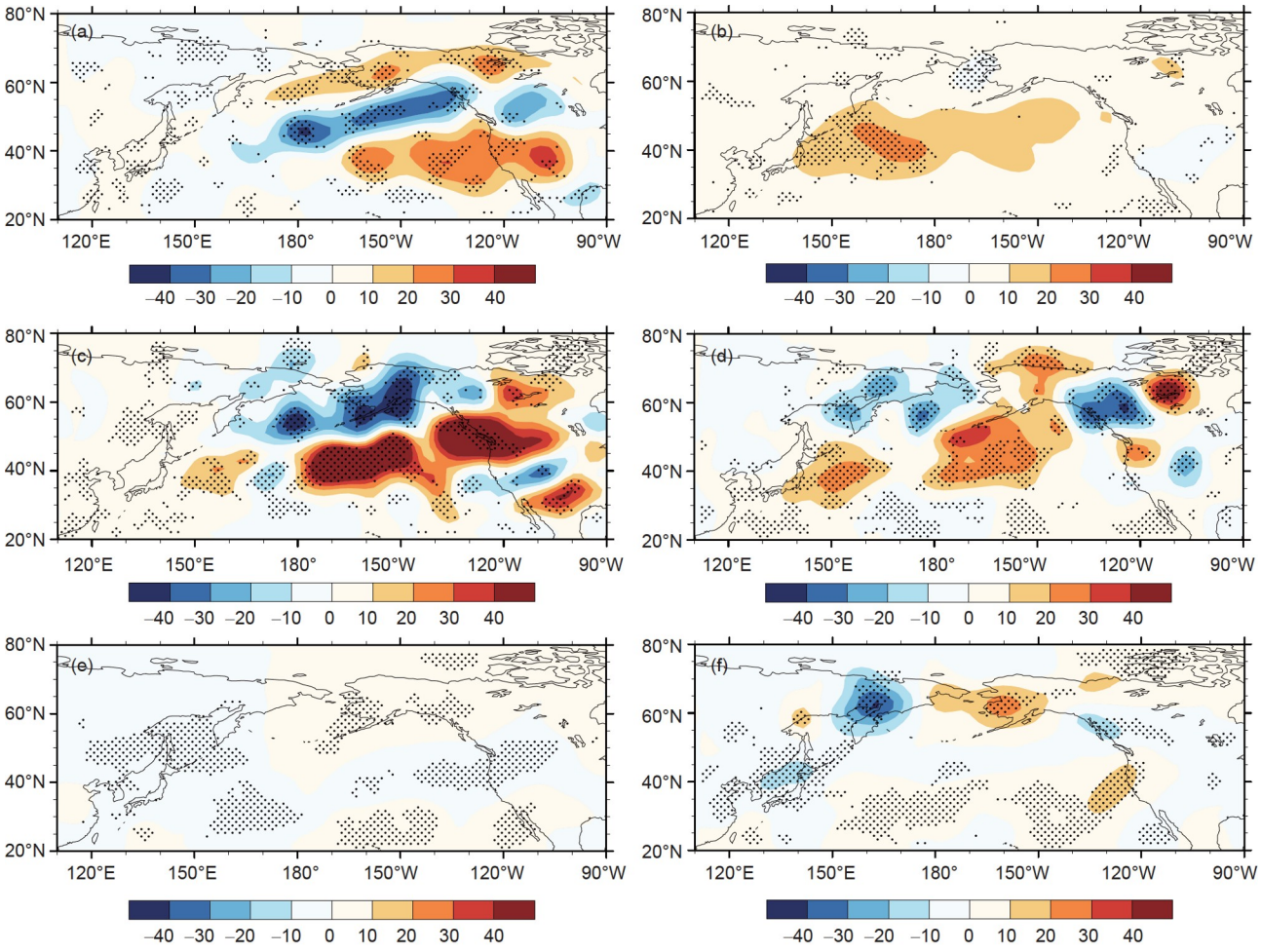


**Figure 10** Response of transient eddy heating to KEDV-M feedback on the geopotential height field at 250 hPa (a) and 850 hPa (b) (shading, unit: $10^{-5}$ m$^2$ s$^{-3}$). Response of transient eddy vorticity to KEDV-M feedback on the geopotential height field at 250 hPa (c) and 850 hPa (d). Response of diabatic heating to KEDV-M feedback on the geopotential height field at 250 hPa (e) and 850 hPa (f) (shading, unit: $10^{-5}$ m$^{-2}$ s$^{-3}$). Statistically significant differences at 90% according to Student's $t$ test are stippled.

mainly in the central-eastern North Pacific (Figure 10c and 10d), and the magnitude is much stronger than the feedback of $F1$. Therefore, the feedback of $F2$ makes a considerable contribution to the geopotential height anomaly, mainly in the central-eastern North Pacific. The feedback of $F3$ on the geopotential height anomaly is shown in Figure 10e and 10f. $F3$ has a very weak feedback on the upper troposphere, and it has weak feedback on the lower troposphere north of 55°N.

*4.2.2 Barotropic energy and baroclinic energy conversion*

From the above analysis, it can be seen that under the influence of the KEDV-M, the synoptic transient eddy feedback mainly produces a strong signal response in the central and eastern North Pacific and may be the main contribution to the geopotential height field in the central and eastern North Pacific. However, the feedback of synoptic transient eddies is weak in the western North Pacific; therefore, the feedback of synoptic transient eddies may not be the main cause of the response of the geopotential height in the western North Pacific. We still analyze the possibility that seasonal-scale, low-frequency anomalies absorb energy from the basic climatological mean flow and become self-sustaining through barotropic energy or baroclinic energy conversion. Under the influence of the KEDV-M, the barotropic energy conversion at 250 hPa in the upper troposphere is shown in Figure 11a. There is a strong barotropic energy conversion on the right side of the jet stream in the western North Pacific, which also indicates that the seasonal low-frequency mode anomaly can continuously absorb kinetic energy from the basic climatological flow and can have self-maintenance. Therefore, the barotropic energy conversion may be one of the reasons for the maintenance of the geopotential height in the western north Pacific. A strong negative anomaly of barotropic energy conversion is found at the outlet of the jet stream in the eastern North Pacific, which indicates that the kinetic energy of the low-frequency mode is continuously converted to the kinetic energy of basic climatological mean flow, and the basic climatological mean flow can be self-maintained, while the low-frequency mode loses its kinetic energy continuously; therefore, other processes must supply the energy of the low-frequency mode, which may be the feedback of synoptic transient eddies. The barotropic energy conversion at 850 hPa in the lower troposphere is almost weak (Figure 11b). The influence of baroclinic energy conversion on the upper troposphere is relatively weak, as shown in Figure 11c. It mainly exists in the eastern North Pacific near the west coast of North America, but its intensity is also relatively weak. Baroclinic energy conversion has significant signals in the lower troposphere, as shown in Figure 11d, which mainly exists in the western and central North Pacific, and there is a significant negative anomaly in the western North Pacific north of 40°N, which indicates that the low-frequency mode can continuously lose its potential energy and convert it to basic climatological mean flow, thus making the low-frequency mode anomaly very weak in the lower troposphere. This may be the main reason why the geopotential height anomaly in the lower troposphere is

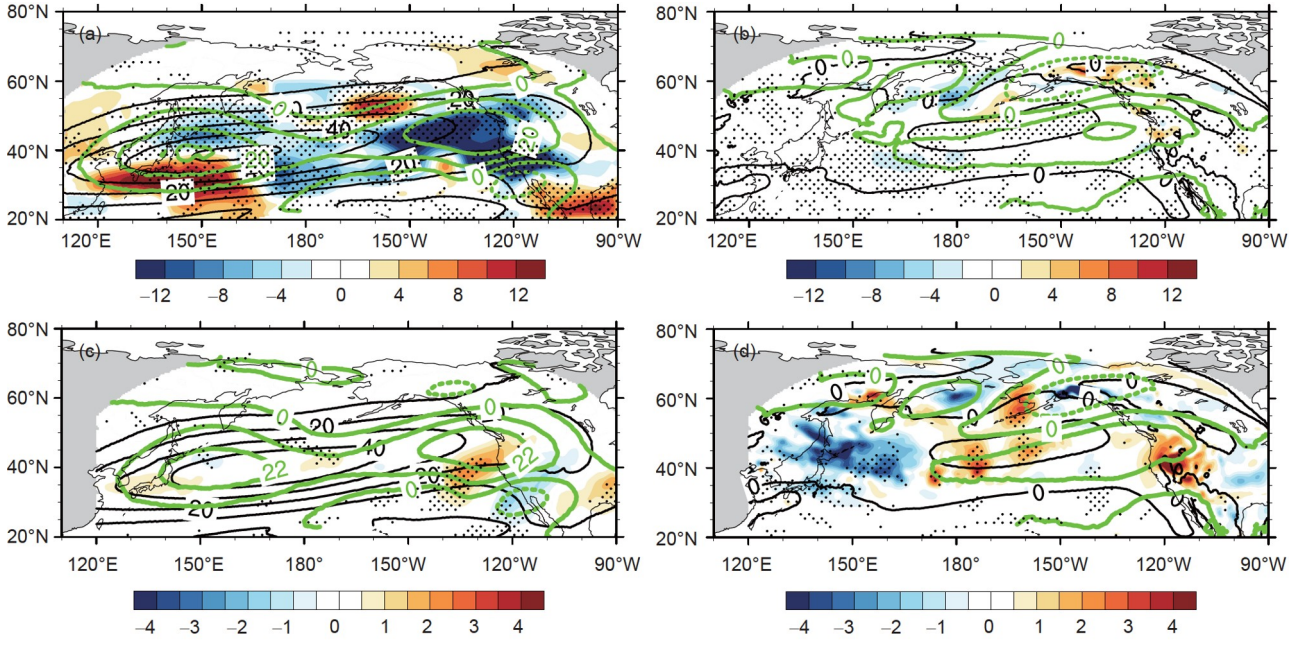


**Figure 11** Response of barotropic and baroclinic energy conversion (shaded, unit: $10^{-4}$ m$^2$ s$^{-3}$) to the KEDV-M. (a) Barotropic energy conversion at 250 hPa and (b) barotropic energy conversion at 850 hPa; (c) and (d) same as (a) and (b) but for baroclinic energy conversion. The black isoline is the climatological zonal wind (unit: m s$^{-1}$), and the green isoline is the response of geopotential height to the mesoscale SSTA (unit: m); statistically significant differences at 90% according to Student's $t$ test are stippled.

weak in the western North Pacific. In general, the barotropic energy conversion in the upper troposphere and baroclinic energy conversion in the lower troposphere are the main factors leading to the geopotential height anomaly in the western North Pacific, which can cause the geopotential height anomaly to have a baroclinic structure with a westward and southward phase tilt with height.

#### *4.2.3 Energy conversion efficiency evaluation*

We still need to understand the relative importance of high-frequency synoptic transient eddy feedback and the interaction between the low-frequency mode and climatological mean flow using energy conversion efficiency. The evaluation results are shown in Figure 12. The barotropic energy conversion has high efficiency in the western North Pacific. The central North Pacific and the eastern North Pacific have high energy conversion efficiency caused by synoptic transient eddies. From the perspective of energy conversion, barotropic energy conversion plays an important role in maintaining large-scale, low-frequency circulation modes in the western North Pacific, while the feedback of synoptic transient eddies in the central and eastern North Pacific plays an important role.

### 4.3 Diagnosis of secondary circulation in the latitude-altitude section

As mentioned above, the meridional propagation of synoptic waves can usually cause the positive feedback of synoptic transient eddies, which can maintain eddy-driven jets by strengthening the meridional convergence of eddy momentum flux (Robinson, 2006; Gerber and Vallis, 2007). In this process, the eddy heat flux drives the baroclinicity shift to the pole, which is accompanied by the formation of secondary circulation in the altitude-latitude section (Vallis, 2006). Under the influence of the KEDV-M, the feedback of the synoptic transient eddy plays an important role. Here, we calculate the secondary circulation in altitude-latitude section caused by the KEDV-M, as shown in Figure 13. Under the influence of the KEDV-M, the counterclockwise secondary circulation in the altitude-latitude section similar to Ferrel circulation is different from that under the influence of the KEDV-L, which may be caused by the feedback of synoptic transient eddy momentum and heat. Under the influence of the KEDV-M, the strong meridional propagation of transient eddy heat flux and momentum flux may induce counterclockwise secondary circulation in the altitude-latitude section with a poleward shift of baroclinicity.

To further diagnose the causes of secondary circulation in the altitude-latitude section and to compare the differences and similarities between the feedback of synoptic transient eddy feedback and diabatic heating on large-scale circulation anomalies, the nonlinear Poisson equation with boundary condition problems of eq. (12) is solved numerically ($\overline{v} = 0$ at the north-south boundary, and $\overline{\omega} = 0$ at the upper and lower boundaries), and the solution results are shown in Figure 14. Under the influence of the KEDV-M, the vertical gradient of EP flux divergence leads to counterclockwise secondary circulation (the first item at the right end of eq. (12)), which is similar to the secondary circulation in the altitude-latitude section under the influence of the KEDV-M; therefore, it may be the main contribution. However, the meridional gradient of diabatic heating has a weak contribution to the secondary circulation in the altitude-latitude section (the second item at the right end of eq. (12)), which indicates the positive feedback of synoptic transient eddies under the influence of the KEDV-M.

## 5. Conclusions

To further explore the influence of different scale SSTA in

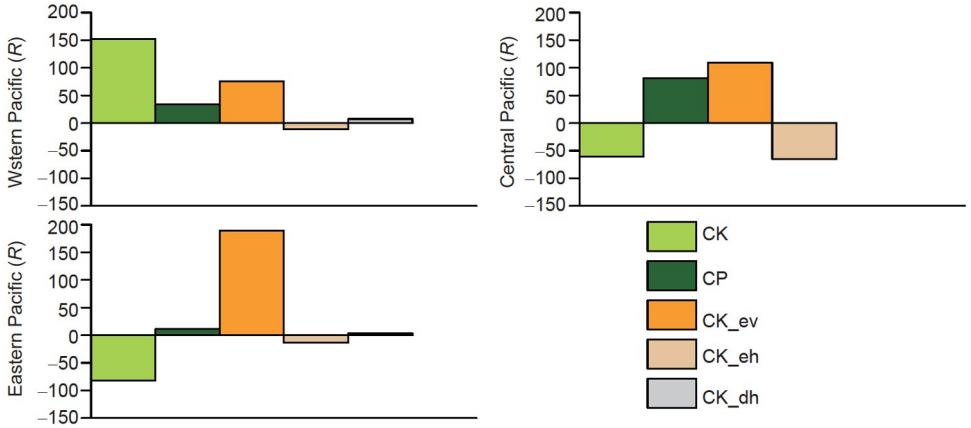


**Figure 12** Energy conversion efficiency *R*. The figure shows the barotropic energy conversion efficiency (CK), baroclinic energy conversion efficiency (CP), energy conversion efficiency caused by transient eddy vorticity feedback (CK_ev), energy conversion efficiency caused by transient eddy heating feedback (CK_eh), and energy conversion efficiency caused by diabatic heating (CP_dh) under the influence of the KEDV-M in the western Pacific, central Pacific and eastern Pacific regions.

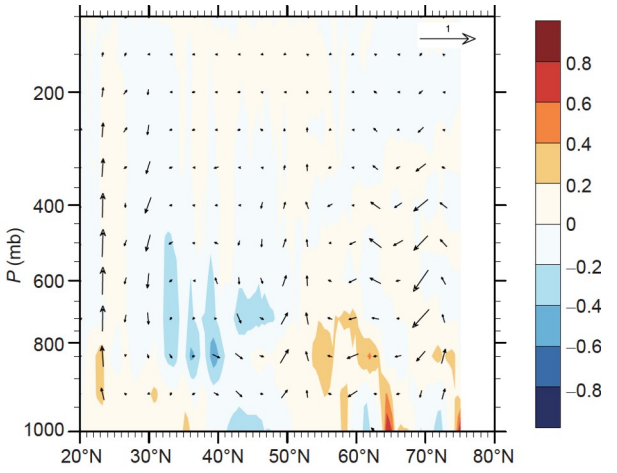


**Figure 13** The response of diabatic heating (unit: K $s^{-1}$) and circulation (vector arrows, meridional wind (unit: 10 m $s^{-1}$) and vertical velocity (unit: $10^{-2}$ m $s^{-1}$)) in latitude-altitude sections to the KEDV-M averaged at 130° E–125°W.

the KEDV-IS on large-scale circulation anomalies and possible mechanisms, this paper uses the regional climate model RegCM4.6 to design three sets of ensemble experiments with different initial values and to obtain the following conclusions.

(1) The response of large-scale circulation in the North Pacific to the KEDV-IS in winter manifests an extensive tripolar structure, which is consistent with the results of a previous analysis. By studying the response of large-scale circulation to different scale SSTA of the KE, it is found that the response of geopotential height with extensive tripolar structure is mainly induced by the KEDV-M, while the geopotential height shows a baroclinic structure under the influence of the KEDV-L in central North Pacific. Using the quasi-geostrophic potential vorticity equation and energy conversion to diagnose and analyze the reasons for maintaining large-scale circulation anomalies, it is found that the large-scale circulation anomalies caused by the KEDV-M are mainly induced by the feedback of synoptic high-frequency transient eddies in the central and eastern North Pacific, while the large-scale circulation anomalies in the western North Pacific can be self-sustained by absorbing kinetic energy from the basic climatological mean flow through barotropic energy conversion. The weak baroclinic atmospheric circulation with weak baroclinic structure in the central North Pacific is mainly caused by diabatic heating under the influence of the KEDV-L, while the feedback of synoptic transient eddies still plays a major role in maintaining atmospheric circulation anomalies in the eastern North Pacific.

(2) The secondary circulation in the altitude-latitude section caused by different scales of the KEDV-IS is obviously different. It can force counterclockwise secondary circulation in the altitude-latitude section similar to Ferrel circulation under the influence of the KEDV-M. While it can force clockwise circulation in the altitude-latitude section, and there is a strong northerly wind anomaly north of 40°N. Through the diagnostic equation of secondary circulation in the altitude-latitude section, it can be found that it strengthens the transportation of momentum and heat by synoptic transient eddies, thus triggering counterclockwise secondary circulation in the altitude-latitude section. However, under the influence of the KEDV-L, the action of diabatic heating can induce clockwise circulation and northerly winds north of 40°N. The above analysis shows that different scales of the KEDV-IS have different influential processes on large-scale atmospheric circulation.

Generally, the feedback of synoptic transient eddies on large-scale circulation (Foussard et al., 2018; Wang et al., 2019) is more important under the influence of the KEDV-M. The feedback of diabatic heating on large-scale atmospheric circulation is more important under the influence of the KEDV-L. Furthermore, it is also noted that the feedback of transient eddies also has some effect on atmospheric circulation under the influence of the KEDV-L, but the reasons for

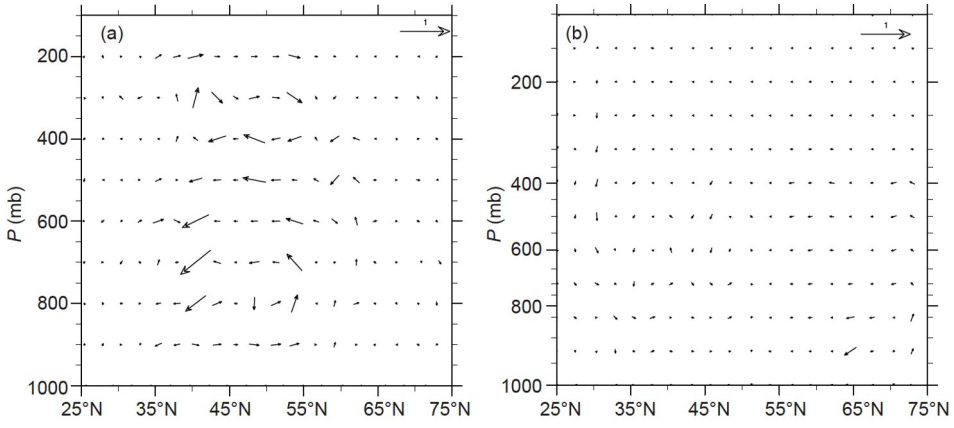


**Figure 14** The latitude-altitude section secondary circulation (meridional velocity (unit: 10 m $s^{-1}$) and vertical velocity (unit: $10^{-2}$ m $s^{-1}$)) caused by eddy momentum and eddy heat flux (a) and diabatic heating (b) under the influence of the KEDV-M.

the enhancement of transient eddies need to be further discussed. Some studies have found that in addition to the ocean front affecting the storm track by changing the baroclinicity in the lower atmosphere, the latent heat provided by large-scale SSTA may still affect the development of the storm track (Businger et al., 2005; Booth et al., 2012; Wang et al., 2019). In this paper, under the influence of the KEDV-L, the enhanced synoptic transient eddy may be the result of sensible and latent heat anomalies caused by large-scale SSTA, which needs to be further studied.

**Acknowledgements** *This work was supported by the National Natural Science Foundation of China (Grant No. 41490642).*

## References

Ahmadi-Givi F. 2002. Areview of the role of latent heat release in extra-tropical cyclones within potential vorticity framework. J Earth Space Phys, 28: 7–20

Alexander M A, Bladé I, Newman M, Lanzante J R, Lau N C, Scott J D. 2002. The atmospheric bridge: The influence of ENSO teleconnections on air-sea interaction over the global oceans. J Clim, 15: 2205–2231

Booth J F, Thompson L A, Patoux J, Kelly K A. 2012. Sensitivity of midlatitude storm intensification to perturbations in the sea surface temperature near the Gulf Stream. Mon Weather Rev, 140: 1241–1256

Businger S, Graziano T M, Kaplan M L, Rozumalski R A. 2005. Cold-air cyclogenesis along the Gulf-Stream front: Investigation of diabatic impacts on cyclone development, frontal structure, and track. Meteorol Atmos Phys, 88: 65–90

Cheng Y H, Ho C R, Zheng Q, Kuo N J. 2014. Statistical characteristics of mesoscale eddies in the North Pacific derived from satellite altimetry. Remote Sens, 6: 5164–5183

Ducet N, Le Traon P Y, Reverdin G. 2000. Global high-resolution mapping of ocean circulation from TOPEX/Poseidon and ERS-1 and -2. J Geophys Res, 105: 19477–19498

Eliassen A, Palm E. 1960. On the transfers of energy in stationary mountain waves. Geophys Publ, 22: 1–23

Fang J B, Yang X Q. 2016. Structure and dynamics of decadal anomalies in the wintertime midlatitude North Pacific ocean-atmosphere system. Clim Dyn, 47: 1989–2007

Foussard A, Lapeyre G, Plougonven R. 2018. Storm track response to oceanic eddies in idealized atmospheric simulations. J Clim, 32: 445–463

Frankignoul C, Müller P, Zorita E. 1997. A simple model of the decadal response of the ocean to stochastic wind forcing. J Phys Oceanogr, 27: 1533–1546

Giorgi F, Coppola E, Solmon F, Mariotti L, Sylla M B, Bi X, Elguindi N, Diro G T, Nair V, Giuliani G, Turuncoglu U U, Cozzini S, Güttler I, O'Brien T A, Tawfik A B, Shalaby A, Zakey A S, Steiner A L, Stordal F, Sloan L C, Brankovic C. 2012. RegCM4: Model description and preliminary tests over multiple CORDEX domains. Clim Res, 52: 7–29

Hadjidimos A. 2000. Successive overrelaxation (SOR) and related methods. J Comput Appl Math, 123: 177–199

Holtslag A A M, Boville B A. 1993. Local versus nonlocal boundary-layer diffusion in a global climate model. J Clim, 6: 1825–1842

Hoskins B J, McIntyre M E, Robertson A W. 1985. On the use and significance of isentropic potential vorticity maps. Q J R Meteorol Soc, 111: 877–946

Joyce T M, Kwon Y O, Yu L. 2009. On the relationship between synoptic wintertime atmospheric variability and path shifts in the Gulf Stream and the Kuroshio Extension. J Clim, 22: 3177–3192

Kalnay E, Kanamitsu M, Kistler R, Collins W, Deaven D, Gandin L, Iredell M, Saha S, White G, Woollen J, Zhu Y, Leetmaa A, Reynolds R, Chelliah M, Ebisuzaki W, Higgins W, Janowiak J, Mo K C, Ropelewski C, Wang J, Jenne R, Joseph D. 1996. The NCEP/NCAR 40-year reanalysis project. Bull Amer Meteorol Soc, 77: 437–471

Lau N C. 1988. Variability of the observed midlatitude storm tracks in relation to low-frequency changes in the circulation pattern. J Atmos Sci, 45: 2718–2743

Lau N C, Nath M J. 1991. Variability of the baroclinic and barotropic transient eddy forcing associated with monthly changes in the midlatitude storm tracks. J Atmos Sci, 48: 2589–2613

Lau N C, Holopainen E O. 1984. Transient eddy forcing of the time-mean flow as identified by geopotential tendencies. J Atmos Sci, 41: 313–328

Lindzen R S, Nigam S. 1987. On the role of sea surface temperature gradients in forcing low-level winds and convergence in the tropics. J Atmos Sci, 44: 2418–2436

Liu Q Y, Wen N, Liu Z Y. 2006. An observational study of the impact of the North Pacific SST on the atmosphere. Geophys Res Lett, 33: L18611

Liu Q Y, Zhang S P, Jia Y L. 2020. Study about ocean eddy effect on strong convection in local atmosphere over the Kuroshio Extension region. Adv Earth Sci, 35: 441–451

Ma X H, Chang P, Saravanan R, Montuoro R, Hsieh J S, Wu D X, Lin X P, Wu L X, Jing Z. 2015. Distant influence of Kuroshio eddies on North Pacific weather patterns? Sci Rep, 5: 17785

Ma X H, Chang P, Saravanan R, Montuoro R, Nakamura H, Wu D X, Lin X P, Wu L X. 2017. Importance of resolving Kuroshio front and eddy influence in simulating the North Pacific storm track. J Clim, 30: 1861–1880

Minobe S, Kuwano-Yoshida A, Komori N, Xie S P, Small R J. 2008. Influence of the Gulf Stream on the troposphere. Nature, 452: 206–209

Nakamura H, Tanaka M, Wallace J M. 1987. Horizontal structure and energetics of Northern Hemisphere wintertime teleconnection patterns. J Atmos Sci, 44: 3377–3391

Nakamura H, Sampe T, Tanimoto Y, Shimpo A. 2004. Observed associations among storm tracks, jet streams and midlatitude oceanic fronts. In: Wang C, Xie S P, Carton J A, eds. Earth's Climate: The Ocean—Atmosphere Interaction. Geophysical Monograph Series. Washington: American Geophysical Union. 329–345

Okajima S, Nakamura H, Nishii K, Miyasaka T, Kuwano-Yoshida A, Taguchi B, Mori M, Kosaka Y. 2018. Mechanisms for the maintenance of the wintertime basin-scale atmospheric response to decadal SST variability in the North Pacific subarctic frontal zone. J Clim, 31: 297–315

O'Reilly C H, Czaja A. 2015. The response of the Pacific storm track and atmospheric circulation to Kuroshio Extension variability. Q J R Meteorol Soc, 141: 52–66

Peng S L, Whitaker J S. 1999. Mechanisms determining the atmospheric response to midlatitude SST anomalies. J Clim, 12: 1393–1408

Qiu B, Chen S M. 2005. Variability of the Kuroshio Extension jet, recirculation gyre, and mesoscale eddies on decadal time scales. J Phys Oceanogr, 35: 2090–2103

Qiu B, Chen S M, Schneider N, Taguchi B. 2014. A coupled decadal prediction of the dynamic state of the Kuroshio Extension system. J Clim, 27: 1751–1764

Révelard A, Frankignoul C, Sennéchael N, Kwon Y O, Qiu B. 2016. Influence of the decadal variability of the Kuroshio Extension on the atmospheric circulation in the cold season. J Clim, 29: 2123–2144

Révelard A, Frankignoul C, Kwon Y O. 2018. A multivariate estimate of the cold season atmospheric response to North Pacific SST variability. J Clim, 31: 2771–2796

Robinson W A. 2006. On the self-maintenance of midlatitude jets. J Atmos Sci, 63: 2109–2122

Sampe T, Nakamura H, Goto A, Ohfuchi W. 2010. Significance of a midlatitude SST frontal zone in the formation of a storm track and an eddy-driven westerly jet. J Clim, 23: 1793–1814

Sun X G, Tao L F, Yang X Q. 2018. The influence of oceanic stochastic forcing on the atmospheric response to midlatitude North Pacific SST

anomalies. Geophys Res Lett, 45: 9297–9304
Taguchi B, Xie S P, Schneider N, Nonaka M, Sasaki H, Sasai Y. 2007. Decadal variability of the Kuroshio Extension: Observations and an Eddy-Resolving Model Hindcast. J Clim, 20: 1459
Taguchi B, Nakamura H, Nonaka M, Komori N, Kuwano-Yoshida A, Takaya K, Goto A. 2012. Seasonal evolutions of atmospheric response to decadal SST anomalies in the North Pacific subarctic frontal zone: Observations and a coupled model simulation. J Clim, 25: 111–139
Tao L F, Yang X Q, Fang J B, Sun X G. 2020. PDO-related wintertime atmospheric anomalies over the midlatitude North Pacific: Local versus remote SST forcing. J Clim, 33: 6989–7010
Vallis G K. 2006. Atmospheric and Ocean Fluid Dynamics: Fundamentals and Large-Scale Circulation. Cambridge: Cambridge University Press
Wallace J M, Mitchell T P, Deser C. 1989. The influence of sea-surface temperature on surface wind in the Eastern Equatorial Pacific: Seasonal and interannual variability. J Clim, 2: 1492–1499
Wang L Y, Hu H B, Yang X Q. 2019. The atmospheric responses to the intensity variability of subtropical front in the wintertime North Pacific. Clim Dyn, 52: 5623–5639
Yao Y, Zhong Z, Yang X Q. 2016. Numerical experiments of the storm track sensitivity to oceanic frontal strength within the Kuroshio/Oyashio Extensions. J Geophys Res-Atmos, 121: 2888–2900
Zeng X B, Zhao M, Dickinson R E. 1998. Intercomparison of bulk aerodynamic algorithms for the computation of sea surface fluxes using TOGA COARE and TAO data. J Clim, 11: 2628–2644
Zhang C, Liu H L, Xie J B, Lin P F, Li C Y, Yang Q, Song J. 2020. North Pacific storm track response to the mesoscale SST in a global high-resolution atmospheric model. Clim Dyn, 55: 1597–1611

(Responsible editor: Lixin WU)